THE ASTROPHYSICAL JOURNAL, 245:357–374, 1981 April 15

X-RAY STUDIES OF QUASARS WITH THE *EINSTEIN* OBSERVATORY. II.

G. ZAMORANI,[1] J. P. HENRY, T. MACCACARO,[1] AND H. TANANBAUM
Harvard-Smithsonian Center for Astrophysics
A. SOLTAN
Copernicus Astronomical Center, Warsaw, Poland
Y. AVNI
Weizmann Institute of Science, Rehovot, Israel
J. LIEBERT, J. STOCKE, P. A. STRITTMATTER, AND R. J. WEYMANN
Steward Observatory, University of Arizona
M. G. SMITH
Royal Observatory, Blackford Hill, Edinburgh
AND
J. J. CONDON
National Radio Astronomy Observatory
and Department of Physics, Virginia Polytechnic Institute and State University
Received 1980 June 9; accepted 1980 October 22

ABSTRACT

Using the *Einstein* Observatory, we have carried out X-ray observations of 107 quasars and have detected 79. From the analysis of this sample of objects we find a correlation between optical emission and X-ray emission. Our data for radio-loud quasars also show a correlation between radio emission and X-ray emission. For a given optical luminosity, the average X-ray emission of radio-loud quasars is ~ 3 times higher than that of radio-quiet quasars. In addition, our data suggest that the ratio of X-ray to optical luminosity is decreasing with increasing redshift and/or optical luminosity. Taking into account the differences in X-ray luminosity between radio-loud and radio-quiet quasars, and between low-redshift and high-redshift quasars, we estimate that $\sim 30\%$ of the observed X-ray background is contributed by quasars brighter than $m_B \approx 20$, while much of the remainder can be contributed by still fainter quasars. Our data also imply that the optical $\log N$–m_B relation for quasars cannot be extrapolated much beyond $m_B \approx 20$ with the steep slope used to characterize optical source counts at brighter magnitudes. This situation supports the picture in which luminosity evolution, rather than pure density evolution, describes the quasar behavior as a function of redshift. We briefly discuss the observed correlation of X-ray luminosity with radio luminosity in the context of current quasar models.

Subject headings: cosmology — quasars — X-rays: sources

I. INTRODUCTION

Einstein observations have clearly established that quasars, as a class, are strong X-ray emitters, at the level of 10^{43}–10^{47} ergs s^{-1} (Tananbaum *et al.* 1979 [Paper I]; Ku 1979). Since these first reports of *Einstein* X-ray observations of quasars, the number of observed and detected objects has more than doubled. The sample we discuss in this paper is composed of both radio-quiet and radio-loud QSOs distributed over the full range of luminosities and redshift. Our sample was constructed according to the following criteria: for the radio-loud QSOs we included quasars selected at both low and high radio frequencies (typical examples are the 3CR and PKS quasars, respectively). In this way, our sample of radio-loud quasars includes both objects with extended radio emission and steep radio spectrum and objects with compact radio emission and flat radio spectrum. Special emphasis was placed on the 3CR quasars as the portion of our original observing program comprising a complete sample. For the radio-quiet QSOs we included both quasars selected on the basis of their color (e.g., PHL) and quasars selected in surveys of emission line objects (e.g., MCS). The large number of objects for which we now have X-ray data and the variety of their radio and optical characteristics allow a first detailed

[1]Also from the Istituto di Radioastronomia, CNR, Bologna, Italy.

study of the X-ray properties as a function of other parameters intrinsic to the quasars (e.g., the radio and optical luminosity) and as a function of evolutionary effects (redshift).

Despite the large number of data we are continuously accumulating, we have not yet completed the observations of any statistically complete sample of radio or optically selected QSOs. For this reason, the correlations which are discussed in the following sections cannot be described in the form of "multivariate" luminosity functions. Also, we do not yet have a complete sample of X-ray discovered quasars large enough for meaningful statistical studies. In order to consider an X-ray QSO as a part of a complete sample, we require that all of the X-ray sources found by chance in a given field have optical identifications down to a selected optical limiting magnitude. So far, only a few of the ~20 CFA X-ray discovered QSOs satisfy this requirement (Giacconi *et al.* 1979; Grindlay *et al.* 1980). For these reasons and in order to exclude the obvious bias in the ratio of X-ray to optical luminosities introduced by the X-ray selection, we have not used the data for the X-ray selected QSOs in the analysis we describe below.

II. THE DATA

As of 1980 February 7 we have observed 107 previously known quasars, detecting 79 of them. Most observations were made with the Imaging Proportional Counter (IPC) on board *Einstein*; High Resolution Imager (HRI) data are available for seven quasars in the sample. In Table 1 we give the relevant X-ray data for the whole sample, including those already published in Paper I. For some of these sources the fluxes and luminosities quoted here are slightly different (but always within the errors) from those previously published. These differences arise because for some of the objects we now have longer observations, and because a different correction has been applied to the observed flux due to the absorption in the Galaxy. Instead of using an average value for the column density of hydrogen ($N_{\rm H}$), we have used for each quasar the appropriate value as derived from the 21 cm radio surveys (Heiles 1975). Also, luminosities quoted in Paper I were based on the counts recorded in the PHA channels corresponding to the emitted energy range 0.5–4.5 keV for each object. The disadvantage of this approach is that, especially for quasars of high redshift, only a fraction of the total net counts is used for computing the flux; the advantage is that the intrinsic luminosities obtained for the fixed energy range are less sensitive to the assumed spectral slope. Now, having more spectral information (see § III*d* for a discussion of this point), we have found that the uncertainties introduced by the assumption of a mean spectrum are, on the average, less important than those introduced by the loss of statistics. For this reason we have used here the largest possible energy range compatible with the instrumental background; thus, for most of the objects observed with the IPC we have used all the net counts recorded in the energy range ~0.25–3.3 keV. We estimate that the current uncertainty in IPC gain combined with the assumption of a mean spectrum can introduce errors of no more than 25% in the calculation of X-ray fluxes (see Paper I for further discussion).

In Table 1 the quasars are listed in order of increasing right ascension. Column (1) gives the source name; column (2) gives the right ascension, declination, and redshift (obtained in most cases from the catalog of Burbidge, Crowne, and Smith 1977; exceptions are referenced in the Table footnote); column (3) gives the column density of hydrogen (atoms $\rm cm^{-2}$) used for the correction to the observed flux due to the absorption in the Galaxy (Heiles 1975), the total exposure time (seconds) for each observation, and the energy range (keV) of the detected photons; column (4) gives the net counts with 1 σ statistical uncertainty, the corresponding observed flux (ergs $\rm cm^{-2}\ s^{-1}$), and the total luminosity (ergs $\rm s^{-1}$) over a fixed energy band, 0.5–4.5 keV, at the source. Both the fluxes and the luminosities have been computed assuming a power law spectrum with energy slope $\alpha_x = 0.5 (S_x \propto \nu^{-\alpha_x})$, and no intrinsic absorption at the source; the luminosities have been computed assuming a Friedmann universe with $H_0 = 50$ km $\rm s^{-1}$ $\rm Mpc^{-1}$ and $q_0 = 0$. (See Paper I for further details.)

Our criteria for source detection were coincidence (within ~1′ for the IPC and ~5″ for the HRI) between the X-ray and optical positions and a net counting rate at least 3 times the standard deviation of the background counting rate in the detection cell. Three sigma upper limits are given for the quasars we did not detect.

In order to compare the X-ray luminosities with the radio and optical luminosities, we have computed the emitted monochromatic luminosities (ergs $\rm s^{-1}$ $\rm Hz^{-1}$) at 2 keV, 2500 Å, 5 GHz (col. [5]). The X-ray luminosity, l_x (2 keV), has been computed from the observed fluxes corrected for absorption in the Galaxy by assuming an X-ray power law spectrum with energy slope $\alpha_x = 0.5$. The optical luminosity, l_0 (2500 Å), has been computed assuming an optical energy slope $\alpha_0 = 1.0$ and using, when available, the U, B, V colors according to the following equations (Wills and Lynds 1978):

$$\log l_0(2500\ \text{Å}) = \begin{cases} 37.735 - 0.4U_c + 2\log A \\ 38.011 - 0.4B_c + 2\log A \\ 37.878 - 0.4V_c + 2\log A, \end{cases} \quad (1)$$

where A, the luminosity distance (Sandage 1961), is $z(1+z/2)$ in a $q_0 = 0$ model, and U_c, B_c, V_c are the U, B, V magnitudes after correction for galactic absorption and the effect of the λ2798 line. We have used Schmidt's (1968) equation (1) and Table 4 for these corrections. For the cases in which all three colors are available, we have used the magnitude with the

TABLE 1

QUASAR OBSERVATIONS

Name (1)	R.A. Decl. Redshift (2)	N_H Time E_1–E_2 (3)	Cts Err Flux L_x (4)	Log l_x Log l_o Log l_r (5)	α_{ox} α_{ro} (6)
3CR 9	00 17 50	1.7E+20	59 16	27.96	1.52
	15 24 16	8733	1.6E−13	31.91	0.68
	2.012	0.18–2.73	8.7E+45	35.57	
PG 0026+129	00 26 38	5.0E+20	504 24	26.91	1.39
	12 59 29	2745	6.2E−12	30.53	<−0.01
	0.142	0.20–2.97	8.0E+44	<30.49	
MCS 275 (1)	00 43 40	3.9E+20	18 6	28.40	1.50
	00 48 06	1851	2.3E−13	32.30	<0.47
	2.210	0.39–2.04	2.4E+46	<34.83	
PHL 891 (2)	00 51 57	3.0E+20	< 54	<27.18	>1.50
	14 39 14	7954	<1.8E−13	31.09	<0.22
	0.874	0.16–2.24	<1.5E+45	<32.29	
PHL 892 (2)	00 52 06	3.0E+20	< 40	<27.03	>1.57
	14 30 31	7954	<1.1E−13	31.10	<0.23
	0.911	0.16–2.24	<1.0E+45	<32.33	
PHL 909 (2)	00 54 32	5.6E+20	421 23	26.76	1.21
	14 29 59	3596	3.4E−12	29.92	<0.14
	0.171	0.15–3.54	5.6E+44	<30.69	
PKS 0112–017 (3)	01 12 44	3.9E+20	328 24	28.12	1.38
	−01 42 54	13527	6.7E−13	31.71	0.62
	1.365	0.32–3.19	1.3E+46	35.05	
0122–379 (4)	01 22 00	3.0E+20	< 27	<28.47	>1.63
	−37 59 00	1553	<4.6E−13	32.71	<0.20
	2.160	0.30–3.20	<2.8E+46	<33.79	
PHL 1027 (5)	01 30 32	3.9E+20	146 16	26.92	1.41
	03 23 44	4006	1.0E−12	30.59	<0.26
	0.363	0.15–3.54	8.1E+44	<31.99	
PHL 1033 (2)	01 31 08	3.9E+20	105 12	26.69	1.06
	03 42 13	4006	1.0E−12	29.45	<0.33
	0.255	0.15–2.72	4.7E+44	<31.22	
3CR 47	01 33 40	5.0E+20	745 29	27.73	1.00
	20 42 16	5790	3.3E−12	30.32	0.70
	0.425	0.20–2.40	5.2E+45	34.10	
PHL 1070 (2)	01 34 43	2.8E+20	46 14	24.72	1.54
	03 23 14	8574	1.6E−13	28.73	<0.25
	0.079	0.32–3.60	5.1E+42	<30.07	
PHL 1092 (2)	01 37 19	4.4E+20	63 15	26.32	1.68
	06 40 10	8817	2.0E−13	30.69	<0.21
	0.396	0.16–3.25	2.0E+44	<31.84	
NAB 0137–010 (6)	01 37 44	3.9E+20	149 16	26.89	1.48
	−01 05 30	3617	1.2E−12	30.75	<0.21
	0.334	0.15–3.56	7.5E+44	<31.89	
MCS 366 (7)	01 43 18	2.8E+20	< 61	<28.62	>1.59
	−01 35 32	7314	<2.2E−13	32.76	<0.47
	3.190	0.23–3.12	<4.1E+46	<35.29	
MCS 368 (7)	01 43 47	2.8E+20	< 33	<28.39	>1.68
	−01 01 28	7044	<1.3E−13	32.78	<0.47
	3.240	0.30–3.48	<2.4E+46	<35.31	
MCS 141 (8)	01 46 44	2.8E+20	< 34	<28.30	>1.82
	01 42 54	7871	<1.4E−13	33.03	<0.20
	2.920	0.27–3.28	<1.9E+46	<34.10	
0205–379 (9)	02 05 24	1.7E+20	48 13	28.30	1.60
	−37 56 00	5545	2.3E−13	32.47	0.35
	2.420	0.32–3.22	1.9E+46	34.35	

TABLE 1 —*Continued*

Name (1)	R.A. Decl. Redshift (2)	N_H Time E_1–E_2 (3)	Cts Err Flux L_x (4)	Log l_x Log l_o Log l_r (5)	α_{ox} α_{ro} (6)
0207−398	02 07 24	2.2E+20	38 12	28.44	1.58
	−39 53 00	4205	2.4E−13	32.57	<0.32
	2.805	0.17−3.48	2.7E+46	<34.27	
3CR 61.1	02 10 49	8.4E+20	11 5	25.76	1.26
	86 05 10	1212	2.6E−13	29.06	0.83
	0.184	0.16−3.36	5.6E+43	33.50	
PHL 1305	02 26 23	2.8E+20	33 8	28.56	1.48
	−03 50 58	1346	6.8E−13	32.42	0.53
	2.064	0.28−3.36	3.6E+46	35.27	
0242−410	02 42 02	2.8E+20	< 84	<27.87	>1.63
	−41 03 40	20987	<1.1E−13	32.11	<0.32
	2.214	0.33−3.22	<7.2E+45	<33.82	
PKS 0312−770 (10)	03 12 56	3.0E+20	257 19	27.01	1.31
	−77 03 01	2140	3.2E−12	30.42	0.46
	0.223	0.25−3.09	9.8E+44	32.90	
3C 110	04 14 49	4.4E+20	341 23	27.90	1.47
	−06 01 04	5815	1.6E−12	31.72	0.45
	0.781	0.25−3.30	7.7E+45	34.12	
0420−388 (4)	04 20 30	3.3E+20	370 31	28.86	1.56
	−38 51 55	23433	4.3E−13	32.93	0.44
	3.120	0.17−3.42	7.0E+46	35.28	
PKS 0424−131	04 24 48	4.5E+20	51 12	27.98	1.66
	−13 09 36	10743	1.4E−13	32.30	0.58
	2.165	0.31−3.13	9.2E+45	35.40	
PKS 0438−436	04 38 43	3.3E+20	22 7	28.87	1.15
	−43 38 52	1266	5.3E−13	31.91	0.87
	2.860	0.27−3.22	7.2E+46	36.57	
3CR 138	05 18 17	2.6E+21	40 9	27.42	1.28
	16 35 26	2823	4.1E−13	30.76	0.82
	0.760	0.26−3.36	2.5E+45	35.19	
PKS 0528−250 (11)	05 28 05	3.9E+20	51 9	28.99	1.34
	−25 05 45	1887	7.6E−13	32.48	0.62
	2.812	0.34−3.39	9.5E+46	35.79	
PKS 0537−441	05 37 21	2.8E+20	18 5	27.80	1.57
	−44 06 40	520	9.6E−13	31.90	0.61
	0.894	0.28−3.33	6.1E+45	35.16	
0537−286 (12)	05 37 57	2.8E+20	723 35	29.22	1.00
	−28 41 27	23831	9.8E−13	31.83	0.72
	3.110	0.16−3.25	1.6E+47	35.72	
3CR 147	05 38 44	2.4E+21	149 23	26.94	1.46
	49 49 43	14549	2.9E−13	30.75	0.82
	0.545	0.27−3.28	8.5E+44	35.18	
PKS 0637−75 (13)	06 37 23	5.0E+20	272 17	28.38	1.25
	−75 13 38	1083	6.9E−12	31.62	0.64
	0.651	0.25−3.09	2.3E+46	35.05	
OH 471	06 42 53	1.3E+21	123 15	29.22	1.44
	44 54 31	5681	6.3E−13	32.95	0.62
	3.400	0.28−3.36	1.6E+47	36.30	
3CR 175	07 10 16	2.0E+21	17 5	27.35	1.67
	11 51 25	1305	3.5E−13	31.69	0.51
	0.768	0.20−3.20	2.2E+45	34.45	
3CR 186	07 40 57	6.1E+20	279 24	27.78	1.38
	38 00 31	14489	5.3E−13	31.38	0.59
	1.063	0.25−3.09	5.9E+45	34.57	

TABLE 1—*Continued*

Name (1)	R.A. Decl. Redshift (2)	N_H Time E_1–E_2 (3)	Cts Err Flux L_x (4)	Log l_x Log l_o Log l_r (5)	α_{ox} α_{ro} (6)
3CR 196	08 09 59	5.0E+20	95 16	27.29	1.43
	48 22 08	9007	3.0E−13	31.02	0.82
	0.871	0.28–3.33	1.9E+45	35.44	
3CR 204	08 33 18	5.0E+20	41 8	27.88	1.26
	65 24 04	1793	6.5E−13	31.16	0.63
	1.112	0.33–3.36	7.4E+45	34.56	
3CR 205	08 35 10	5.6E+20	185 22	28.00	1.46
	58 04 52	14038	3.7E−13	31.82	0.65
	1.534	0.27–3.25	9.7E+45	35.30	
3CR 207	08 38 02	5.0E+20	385 26	27.48	1.22
	13 23 05	13565	7.8E−13	30.66	0.72
	0.684	0.25–3.11	2.9E+45	34.55	
3CR 208	08 50 23	3.9E+20	23 6	27.79	1.42
	14 03 58	1465	4.0E−13	31.48	0.64
	1.110	0.31–2.32	5.9E+45	34.92	
3CR 215	09 03 44	3.9E+20	610 31	27.16	1.15
	16 58 16	13629	1.2E−12	30.17	0.65
	0.411	0.25–3.11	1.4E+45	33.67	
4C 39.25	09 23 56	1.7E+20	935 35	27.93	1.14
	39 15 23	10268	2.5E−12	30.89	0.77
	0.699	0.28–3.36	8.3E+45	35.02	
MC5 0938+1159 (14).....	09 38 32	3.9E+20	< 83	<28.45	>1.38
	11 59 13	14728	<1.6E−13	32.04	0.60
	3.183	0.16–3.33	<2.7E+46	35.28	
4C 13.41	10 04 45	3.9E+20	< 20	<26.16	>1.82
	13 03 38	1378	<4.1E−13	30.91	0.43
	0.240	0.16–3.39	<1.4E+44	33.21	
3C 243 (HRI)	10 23 55	3.0E+20	< 6	<28.05	>1.38
	06 43 32	1678	<4.5E−13	31.65	0.62
	1.699	0.10–4.50	<1.1E+46	35.00	
1028+313	10 28 10	2.2E+20	1260 39	26.96	1.12
	31 18 21	6457	5.5E−12	29.88	0.48
	0.177	0.18–3.58	8.8E+44	32.45	
1054−034	10 54 10	3.9E+20	50 13	27.59	1.71
	−03 24 39	23205	7.0E−14	32.03	<0.47
	2.100	0.29–3.55	3.8E+45	<34.57	
3CR 249.1	11 00 27	3.9E+20	215 18	27.25	1.44
	77 15 09	2064	2.9E−12	31.00	0.49
	0.311	0.20–3.27	1.7E+45	33.63	
3CR 263	11 37 09	1.7E+20	277 20	27.99	1.30
	66 04 27	2179	3.4E−12	31.37	0.58
	0.652	0.20–3.30	9.6E+45	34.48	
GQ Com	12 02 09	2.8E+20	1138 36	27.04	1.30
	28 10 54	4335	7.5E−12	30.42	<0.30
	0.165	0.18–3.58	1.1E+45	<32.03	
PKS 1207−399 (10)	12 07 00	8.4E+20	22 7	27.65	1.51
	−39 59 31	1297	4.7E−13	31.58	0.53
	0.966	0.30–3.05	4.3E+45	34.43	
PKS 1217+023	12 17 38	2.8E+20	758 29	27.43	1.14
	02 20 21	2488	8.6E−12	30.40	0.50
	0.240	0.14–3.68	2.6E+45	33.08	
Mrk 205 (15) (HRI)	12 19 34	3.0E+20	367 19	26.47	1.25
	75 35 15	4437	1.7E−11	29.74	−0.06
	0.070	0.10–4.50	2.9E+44	29.43	

TABLE 1—*Continued*

Name (1)	R.A. Decl. Redshift (2)	N_H Time E_1–E_2 (3)	Cts Err Flux L_x (4)	Log l_x Log l_o Log l_r (5)	α_{ox} α_{ro} (6)
4C 25.40	12 23 09	3.3E+20	77 12	26.53	1.53
	25 15 12	2668	7.9E−13	30.52	0.39
	0.268	0.16−3.33	3.3E+44	32.60	
B2 1225+31 (16)	12 25 56	2.2E+20	211 19	28.70	1.62
	31 45 13	6918	8.6E−13	32.93	0.37
	2.200	0.18−3.58	4.8E+46	34.95	
3CR 273(HRI)	12 26 33	3.0E+20	68512 262	28.24	1.22
	02 19 42	75240	1.5E−10	31.41	0.60
	0.158	0.10−4.50	1.7E+46	34.63	
PKS 1237−101	12 37 07	3.9E+20	25 7	27.33	1.40
	−10 07 01	1454	4.8E−13	30.99	0.66
	0.753	0.26−3.36	2.1E+45	34.54	
KP 1243.7+34.6 (5)	12 43 45	2.2E+20	< 30	<28.08	>1.25
	34 37 25	6029	<1.8E−13	31.33	<0.52
	2.290	0.15−3.27	<1.2E+46	<34.12	
KP 1244.0+34.5 (5)	12 44 05	2.2E+20	< 32	<27.88	>1.24
	34 33 05	6029	<1.7E−13	31.11	<0.44
	1.940	0.15−3.27	<7.4E+45	<33.50	
KP 1244.1+34.6 (5)	12 44 09	2.2E+20	< 55	<28.23	>1.17
	34 41 04	6029	<2.7E−13	31.28	<0.50
	2.200	0.15−3.27	<1.6E+46	<33.95	
KP 1244.2+34.6 (5)	12 44 14	2.2E+20	< 63	<28.30	>1.23
	34 40 55	6029	<3.1E−13	31.50	<0.43
	2.240	0.15−3.27	<1.9E+46	<33.83	
KP 1244.9+34.7 (5)	12 44 57	2.2E+20	< 38	<28.18	>1.56
	34 43 54	6029	<1.8E−13	32.24	<0.34
	2.490	0.15−3.27	<1.5E+46	<34.08	
B19	12 45 03	2.2E+20	< 61	<28.19	>1.50
	34 31 31	6029	<2.9E−13	32.09	<0.31
	2.070	0.15−3.27	<1.5E+46	<33.74	
KP 1245.3+34.3 (5)	12 45 20	2.2E+20	< 40	<27.96	>1.15
	34 18 27	6029	<2.9E−13	30.95	<0.51
	1.700	0.15−3.27	<8.8E+45	<33.69	
KP 1245.6+34.2 (5)	12 45 39	2.2E+20	< 28	<27.67	>1.18
	34 16 36	6029	<1.5E−13	30.75	<0.34
	1.700	0.15−3.27	<4.5E+45	<32.61	
KP 1246.0+34.4 (5)	12 46 06	2.2E+20	< 30	<28.06	>1.40
	34 29 00	6029	<1.8E−13	31.70	<0.40
	2.230	0.15−3.27	<1.1E+46	<33.87	
B46	12 46 30	2.2E+20	79 14	26.33	1.33
	34 40 49	6029	4.9E−13	29.80	<0.35
	0.271	0.15−3.27	2.1E+44	<31.69	
KP 1246.5+34.6 (5)	12 46 31	2.2E+20	< 76	<28.29	>1.38
	34 41 16	6029	<4.8E−13	31.87	<0.32
	1.880	0.15−3.27	<1.9E+46	<33.62	
1246−057	12 46 38	3.9E+20	< 31	<28.19	>1.70
	−05 42 44	3568	<2.2E−13	32.63	<0.41
	2.212	0.32−3.22	<1.5E+46	<34.83	
PKS 1252+119	12 52 08	2.8E+20	79 11	27.78	1.43
	11 57 21	2305	9.1E−13	31.50	0.57
	0.871	0.24−3.04	5.8E+45	34.59	
3C 279	12 53 36	3.9E+20	530 25	28.04	0.97
	−05 31 08	2926	5.1E−12	30.56	0.86
	0.538	0.27−3.10	1.1E+46	35.20	

TABLE 1—*Continued*

Name (1)	R.A. Decl. Redshift (2)	N_H Time E_1–E_2 (3)	Cts Err Flux L_x (4)	Log l_x Log l_o Log l_r (5)	α_{ox} α_{ro} (6)
1300−243 (15)	13 00 37	8.4E+20	< 17	<28.40	>1.47
	−24 18 56	1348	<3.3E−13	32.22	<0.49
	2.259	0.20−3.36	<2.5E+46	<34.85	
1309−056 (15)	13 09 01	3.9E+20	28 8	28.46	1.54
	−05 36 43	1604	4.8E−13	32.48	<0.30
	2.180	0.18−3.54	2.8E+46	<34.08	
TON 155 (2).....	13 18 54	2.2E+20	40 10	28.15	1.55
	29 03 30	2629	4.5E−13	32.19	<0.20
	1.703	0.22−3.36	1.4E+46	<33.29	
TON 156 (2) (HRI)	13 18 55	2.2E+20	< 12	<26.63	>1.71
	29 03 00	6100	<2.6E−13	31.08	<0.18
	0.549	0.10−45.0	<4.2E+44	<32.06	
MC3 1331+170	13 31 10	2.2E+20	33 9	28.35	1.71
	17 04 24	2235	3.9E−13	32.81	0.37
	2.081	0.24−3.04	2.2E+46	34.82	
RS 23	13 34 36	1.7E+20	< 29	<28.16	>1.32
	28 35 42	2089	<3.8E−13	31.60	<0.31
	1.910	0.24−3.67	<1.4E+46	<33.29	
3CR 288.1	13 40 30	2.2E+20	40 13	27.14	1.48
	60 36 48	5468	2.0E−13	30.99	0.67
	0.961	0.14−3.51	1.3E+45	34.57	
1346−036 (15)	13 46 08	3.9E+20	< 54	<28.34	>1.57
	−03 38 31	5731	<2.7E−13	32.43	<0.46
	2.344	0.28−3.31	<2.1E+46	<34.90	
PG 1351+64.....	13 51 46	2.6E+20	22 9	25.14	1.87
	64 00 28	1898	3.5E−13	30.02	0.22
	0.088	0.18−3.51	1.4E+43	31.19	
PKS 1402+044 (17)	14 02 30	3.3E+20	32 16	28.26	1.59
	04 29 55	9713	7.9E−14	32.40	0.60
	3.200	0.16−2.46	1.8E+46	35.61	
3CR 298	14 16 39	2.5E+20	59 11	28.04	1.52
	06 42 21	2198	6.0E−13	32.00	0.67
	1.439	0.20−3.36	1.1E+46	35.60	
PKS 1422+202	14 22 38	2.8E+20	30 7	27.52	1.33
	20 13 57	1635	5.1E−13	30.98	0.67
	0.871	0.32−3.19	3.2E+45	34.58	
3CR 309.1	14 58 58	2.8E+20	123 13	27.88	1.38
	71 52 12	3009	1.1E−12	31.49	0.71
	0.905	0.28−309	7.4E+45	35.32	
4C 10.43	15 24 22	3.9E+20	21 9	27.70	1.45
	10 09 32	2621	2.7E−13	31.49	0.50
	1.358	0.24−3.21	4.9E+45	34.19	
KP 1548.3+1136 (5) (HRI).	15 48 20	3.9E+20	< 8	<28.41	>1.04
	11 36 15	2200	<7.3E−13	31.13	<0.42
	1.920	0.10−4.50	<2.5E+46	<33.40	
1548+115A (18).....	15 48 21	3.9E+20	270 19	27.47	1.21
	11 29 47	3324	2.3E−12	30.63	0.54
	0.436	0.33−3.36	2.9E+45	33.56	
1548+115B (18) (HRI)	15 48 22	3.9E+20	< 30	<28.80	>1.12
	11 29 46	2361	<1.9E−12	31.72	<0.31
	1.901	0.10−4.50	<6.2E+46	<33.41	
GC 1555+33.....	15 55 33	3.3E+20	19 8	27.17	1.42
	33 13 25	5088	2.0E−13	30.88	0.55
	0.942	0.36−3.52	1.4E+45	33.83	

TABLE 1—*Continued*

Name (1)	R.A. Decl. Redshift (2)	N_H Time E_1–E_2 (3)	Cts Err Flux L_x (4)	Log l_x Log l_o Log l_r (5)	α_{ox} α_{ro} (6)
GC 1556+335	15 56 59	3.3E+20	41 11	27.83	1.65
	33 31 47	5088	2.2E−13	32.13	0.43
	1.650	0.36–3.52	6.6E+45	34.43	
MC2 1635+119	16 35 26	6.1E+20	299 21	26.45	1.21
	11 55 41	3894	2.2E−12	29.59	0.41
	0.146	0.26–3.36	2.7E+44	31.81	
KP 1703.5+609 (5)	17 03 28	2.8E+20	34 10	28.39	1.46
	60 51 55	1985	4.9E−13	32.20	<0.45
	1.980	0.20–3.20	2.4E+46	<34.60	
3CR 351	17 04 04	2.8E+20	74 12	26.98	1.66
	60 48 29	1985	1.0E−12	31.31	0.50
	0.371	0.40–3.20	9.3E+44	33.98	
V396 Her	17 20 38	7.2E+20	16 6	26.07	1.55
	24 39 06	857	6.6E−13	30.11	<0.32
	0.175	0.28–3.75	1.1E+44	<31.80	
1803+676	18 03 36	6.1E+20	507 26	26.42	1.36
	67 37 00	5991	2.4E−12	29.96	<0.50
	0.136	0.17–3.45	2.6E+44	<32.64	
3CR 380	18 28 13	6.1E+20	145 13	27.96	1.30
	48 42 39	1692	2.4E−12	31.33	0.74
	0.692	0.17–3.36	8.8E+45	35.32	
PKS 2126−150 (10)	21 26 27	6.1E+20	471 24	29.77	1.22
	−15 51 52	4923	2.6E−12	32.94	0.55
	3.270	0.24–3.01	5.8E+47	35.90	
PHL 1657	21 35 01	3.0E+20	324 19	27.23	1.30
	−14 46 27	1342	7.1E−12	30.63	0.51
	0.200	0.25–3.51	1.7E+45	33.39	
OX 169 (HRI)	21 41 13	8.4E+20	46 7	26.21	1.68
	17 29 49	14398	6.9E−13	30.58	0.44
	0.213	0.10–4.50	1.6E+44	32.97	
2204−408 (4)	22 04 33	3.9E+20	43 14	28.52	1.61
	−40 51 35	7104	1.7E−13	32.73	0.35
	3.180	0.25–3.11	3.2E+46	34.61	
3C 446	22 23 11	6.1E+20	230 16	29.00	0.91
	−05 12 17	1379	4.7E−12	31.37	0.80
	1.404	0.16–3.39	9.6E+46	35.70	
PHL 5200	22 25 54	2.8E+20	< 27	<28.53	>1.36
	−05 34 17	1063	<7.1E−13	32.08	<0.33
	1.981	0.37–3.58	<3.3E+46	<33.86	
CTA 102	22 30 07	6.1E+20	252 18	28.33	1.18
	11 28 23	3853	2.0E−12	31.41	0.75
	1.037	0.31–3.21	2.1E+46	35.45	
PKS 2254+024	22 54 45	5.0E+20	73 17	28.00	1.55
	02 27 12	12161	1.6E−13	32.03	0.55
	2.090	0.31–3.21	9.8E+45	35.01	
4C 09.74	23 44 04	6.1E+20	52 8	27.79	1.44
	09 14 05	887	1.7E−12	31.53	0.55
	0.677	0.28–3.36	5.9E+45	34.47	
2357−348	23 57 06	2.8E+20	68 14	28.27	1.59
	−34 51 53	5301	3.5E−13	32.40	<0.44
	2.070	0.16–3.36	1.8E+46	<34.75	

REFERENCES.—(1) MacAlpine, Lewis, and Smith 1977. (2) Fanti *et al.* 1977. (3) Wills and Lynds 1978. (4) Osmer and Smith 1977*b*. (5) Sramek and Weedman 1978. (6) Margon 1977. (7) MacAlpine and Lewis 1978. (8) MacAlpine, Smith, and Lewis 1977. (9) Osmer and Smith 1977*c*. (10) Jauncey *et al.* 1978*a*. (11) Jauncey *et al.* 1978*b*. (12) Wright *et al.* 1978. (13) Adam 1978. (14) Osmer and Smith 1977*a*. (15) Nieto 1978. (16) Bergamini *et al.* 1973. (17) Peterson *et al.* 1978. (18) Argue *et al.* 1974.

filter closest to $2500(1+z)$ Å. The radio luminosity, l_r (5 GHz), has been computed using the following equation:

$$\log l_r(5\text{ GHz}) = 34.63 + \log S(\nu) + 2\log A + \alpha_r \log \frac{\nu}{5000} + (\alpha_r - 1)\log(1+z), \quad (2)$$

where $S(\nu)$ is the observed flux (in janskys) at frequency ν and α_r is the energy slope measured at radio wavelength. Most of the radio data have been obtained from an updated version of the Ohio Master List of Radio Sources. When only measurements at one frequency or only upper limits are available, we have assumed $\alpha_r = 0.7$. (Note that the exact value for α_r is not critical for the results discussed below.) When an actual value for α_r is available, l_r (5 GHz) has been computed using the measured α_r. In order to compare radio luminosities for all of the observed quasars and to avoid restricting our discussion to only those objects which have been observed with very high spatial resolution, we have used the total radio flux for each source.

The last column of Table 1 gives the nominal power law energy slope between the radio and optical bands (α_{ro}) and between the optical and X-ray bands (α_{ox}). Since the emitting regions at different wavelengths may have different physical extents, which we have not taken into account with our use of total fluxes, the spectral indices in Table 1 should be considered only as useful indicators of the distribution of the total energy output as a function of energy.

III. DATA ANALYSIS

a) Correlation between the X-ray and Optical Fluxes

We have first looked for a correlation between the optical and the X-ray emission. As already noted in Paper I, the observed distribution of α_{ox} is broad. Using only the values of the 79 X-ray detections, we find $\sigma(\alpha_{ox}) \approx 0.20$; this means that, within $\pm 1\ \sigma$, the ratio of optical to X-ray luminosity (l_o/l_x) varies by about a factor 10. The entire range of observed $\alpha_{ox}(0.91, 1.87)$ corresponds to a range of ~ 300 in l_o/l_x. Fig. 1 shows the 0.25–3.3 keV X-ray flux (S_x) versus the blue magnitude (m_B) for the total sample of 107 quasars. The data have not been K-corrected to correspond to fixed wavebands at the sources in order to avoid the introduction of additional uncertainties due to the lack of information on optical and X-ray spectral indices for some of the sources. Despite the large dispersion of the points, a significant correlation is present. Using only the detections and excluding 3C 273, we obtain the two regression lines shown in Figure 1, corresponding to the regression of S_x on m_B and m_B on S_x. From the observed correlation coefficient ($r = 0.45$) and the total number of points ($N = 78$) we find that the observed distribution could arise by chance from a sample in

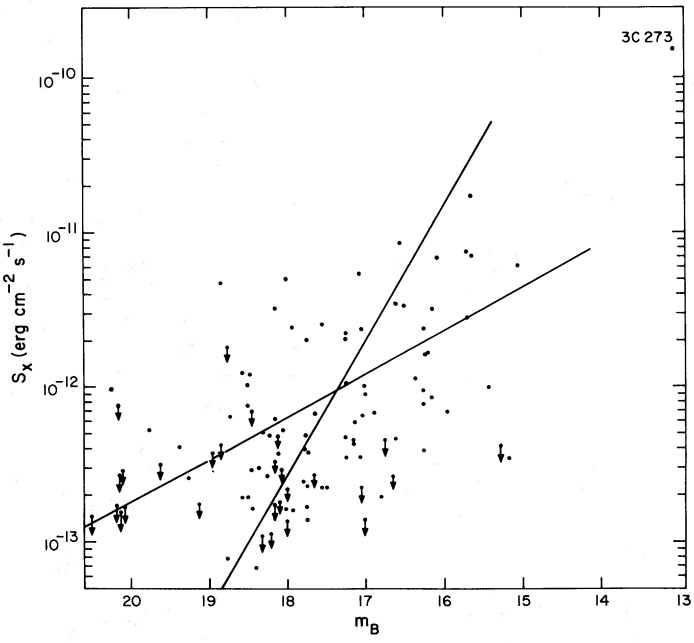

FIG. 1.—Observed X-ray flux (~0.25–3.3 keV) versus blue magnitude for our sample of 107 quasars (79 X-ray detections and 28 X-ray upper limits). The two straight lines represent the two regression lines obtained using the detections only (and excluding 3C 273).

which the optical and X-ray fluxes are uncorrelated with a probability of $\sim 2\times 10^{-5}$. (The inclusion of 3C 273 would decrease this probability to $\sim 10^{-7}$.)

For flux-limited samples, a search for correlations between fluxes has the advantage of avoiding the problem of introducing spurious correlations between luminosities when distance corrections are applied. At the same time, it is also possible for uncorrelated luminosity distributions to show flux correlations under special circumstances. To check for this possibility, we have used the observed optical and X-ray luminosity distributions to estimate the expected $\sigma(\alpha_{ox})$ under the hypothesis that no correlation between l_o and l_x is present. The value of $\sigma(\alpha_{ox})$ obtained in this way (0.44) is substantially higher than the observed value (0.20), supporting the conclusion of a positive correlation between l_x and l_o.

b) Correlation of α_{ox} with the Radio Emission

Figure 2 shows the distribution of α_{ro} for our sample of 107 quasars. Sources with positive radio detections are shown in the lower part, and those with radio upper limits in the upper part. In the following discussion we have defined as "radio loud" quasars all of the radio detected QSOs with $\alpha_{ro}>0.35$; all the others have been considered "radio quiet," including two objects with positive radio detections and $\alpha_{ro}<0.35$ ($\alpha_{ro}=0.35$ corresponds approximately to $\log R=1.9$ in the notation used by Sramek and Weedman 1980). It is evident from Figure 2 that the only substantial objection to this operational definition might arise for those 18 objects for which we have radio upper limits in the range $\alpha_{ro}=0.35$–0.55. However, on the basis of the bivariate (radio-optical) luminosity function for optically selected quasars (Fanti *et al.* 1977; Sramek and Weedman 1978, 1980), we expect that $\lesssim 15\%$ of these objects would satisfy our definition for "radio loud." Thus we expect a misclassification for only one or two objects. This result is supported by a recent radio survey at 5.0 and 14.5 GHz of a sample of 122 optically selected QSOs (Smith and Wright 1980). Only 10% of the objects (with typical optical magnitudes $m\approx 18\pm 1$) were detected as radio sources above a flux density of 20 mJy (corresponding to $\alpha_{ro}\approx 0.3\pm 0.1$).

Using these definitions, our sample is composed of 45 radio-quiet and 62 radio-loud quasars. For the radio-quiet we have 20 X-ray detections (44%); for the radio-loud, 59 X-ray detections (95%). As the ranges of optical magnitudes and X-ray limiting sensitivities are similar for the two samples, the large difference in the rate of X-ray detections gives a first suggestion of difference between the two samples. A more quantitative conclusion on this difference can be reached by computing the maximum likelihood probability distributions of α_{ox} for the two samples (Avni *et al.* 1980) and then comparing the two distributions.

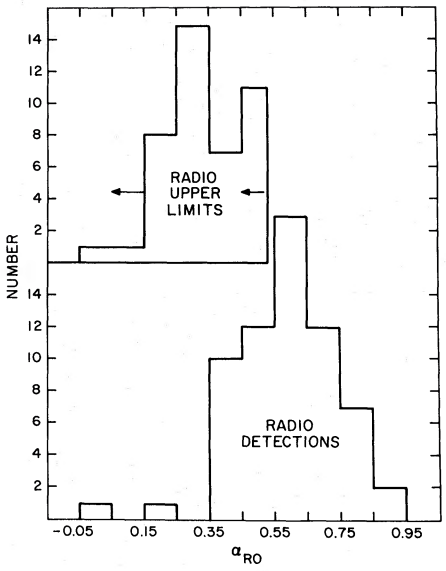

FIG. 2.—Distribution of the spectral index between radio and optical frequencies (α_{ro}). In the upper part, we have plotted the radio upper limits; in the lower part, the radio detections.

Figures 3*a* and 3*b* show the differential and integral distributions of α_{ox} for the radio loud and radio-quiet QSOs, obtained after having taken into proper account both the detections and the upper limits. By analogy with the notation generally used in studying the bivariate radio-optical luminosity function (Schmidt 1972; Fanti *et al.* 1973) we have adopted the symbols $\Psi(\alpha_{ox})$ and $G(<\alpha_{ox})$, which represent the fraction of objects having a spectral index between optical and X-ray frequencies equal to any given value [$\Psi(\alpha_{ox})$, differential distribution] and smaller than any given value [$G(<\alpha_{ox})$, integral distribution]. In Figure 3*a*, the dashed arrow in the radio-loud histogram corresponds to a value of α_{ox} where, having only one upper limit and no detection, we cannot obtain a reliable estimate of the true probability distribution. For Figure 3*a* the data were binned in steps of 0.1 in α_{ox}, while for Figure 3*b* the data were binned in steps of 0.02 in α_{ox}.

The difference between the two distributions is evident in the integral representation of Figure 3*b*: the probability of finding an X-ray source stronger than any given value of α_{ox} is higher for the radio-loud quasars than for the radio-quiet. The shapes of the two integral distributions appear similar to each other, but their systematic displacement is such that the average ratio l_x/l_o for radio-loud is ~ 3 times higher than the same ratio for radio-quiet quasars. (See the discussion at the end of this section for qualifications of these statements.)

It is not straightforward to compute the significance of the observed difference, essentially because the two distributions have already been statistically corrected in order to take into account the presence of some upper limits. One of the most powerful tests for the compari-

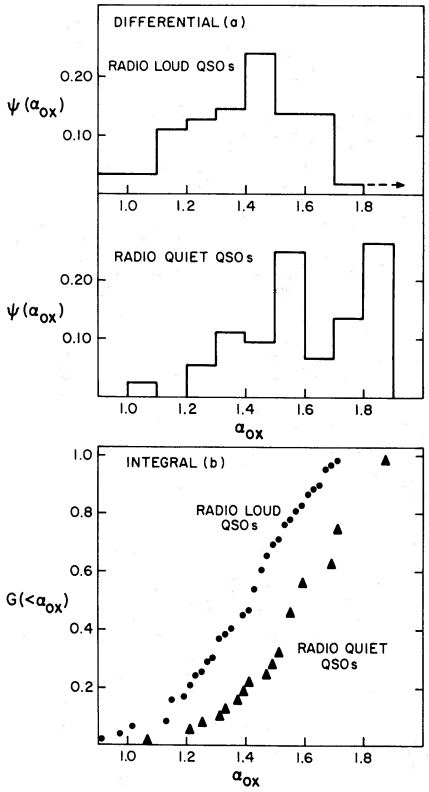

FIG. 3.—Maximum likelihood probability distributions of α_{ox} for the radio loud and radio quiet quasars in (*a*) differential and (*b*) integral form. See text for the description of the technique used for obtaining the maximum likelihood probability distributions.

son of two samples is the Kolmogorov-Smirnov (K-S) test (Kendall and Stuart 1961), which is sensitive to *any* type of difference in the two distributions. This test can be rigorously applied only to samples without upper limits, so that its application in this case requires some modification. The Appendix presents a detailed description of a Monte Carlo simulation which we have carried out. This calculation allows us to determine the proper statistical significance of the difference measured by the K-S test for our specific distributions corrected for the presence of upper limits. The application of this modified K-S test to the two α_{ox} distributions of Figure 3 gives a probability $\sim 5\times 10^{-4}$ that the two distributions are drawn from the same parent population.

In Paper I we introduced the quantity $\alpha_{ox}^{\rm eff}$ which is the spectral index corresponding to the average ratio of X-ray to optical luminosity. The value of this index is strongly dependent on those quasars with a high ratio of X-ray to optical luminosity, and as a result the value of $\alpha_{ox}^{\rm eff}$ is not a full measure of the overall distribution. At the same time, Avni *et al.* (1980) discuss the rigorous calculation of the uncertainty in $\alpha_{ox}^{\rm eff}$ even when upper limits have been used to obtain the maximum likelihood probability distribution. Following the calculations of Avni *et al.* we compute $\alpha_{ox}^{\rm eff}=1.27\pm0.03$ for the radio-loud quasars and $\alpha_{ox}^{\rm eff}=1.46^{+0.05}_{-0.07}$ for the radio-quiet quasars. The difference in $\alpha_{ox}^{\rm eff}$ for these two samples is 0.19 ± 0.076, which yields a probability of $\sim 1\%$ that the two $\alpha_{ox}^{\rm eff}$ are the same.

In order to further study this correlation *within* the sample of radio-loud quasars, we have plotted in Figure 4 the distribution of α_{ro} versus α_{ox} for the sample of 62 radio-loud quasars. In the lower right corner we have indicated the region occupied by the radio-quiet QSOs. This figure shows the presence of a definite correlation, although with large dispersion, between α_{ro} and α_{ox}. The significance level obtained through a linear regression analysis applied to the 59 X-ray detections is 10^{-5}.

We can exclude the possibility that the α_{ro}–α_{ox} correlation is artificially introduced through the presence of l_o in the definition of both quantities (Kembhavi and Fabian 1980). This is accomplished by observing directly the correlation between l_x and l_r (significance level of 10^{-6}) as well as the correlation between monochromatic X-ray and radio fluxes (significance level of 1.5×10^{-3} excluding 3C 273). Anticipating results which are discussed in the next subsection (§ III*c*), we have also evaluated the possibility that the α_{ro}–α_{ox} correlation is a result of correlation of α_{ox} with l_o and/or z. We have considered a restricted range of l_o ($30.0\leq\log l_o\leq 32.0$) for the radio-loud quasars. For this subsample (45 objects) there is no correlation between α_{ro} and l_o, yet the α_{ro}–α_{ox} correlation is still significant at the 5×10^{-4} level. The absence of a significant correlation of α_{ox} with z for the radio-loud quasars shows that such a

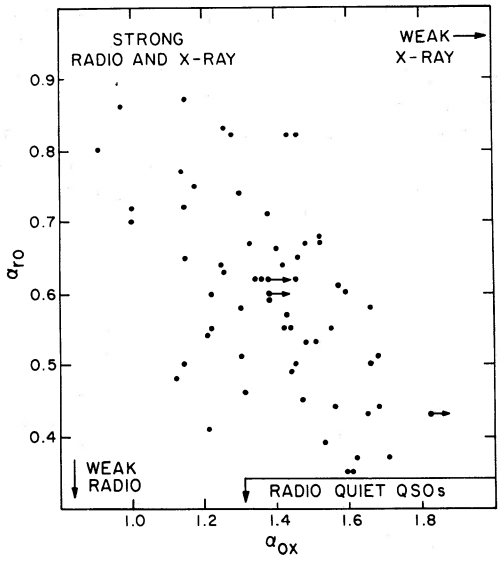

FIG. 4.—α_{ro} versus α_{ox} for our sample of 62 radio loud quasars. Directions are indicated for decreasing radio emission and decreasing X-ray emission. More than 90% of the radio-quiet quasars have α_{ox} within the region bracketed at the bottom of the figure.

redshift effect cannot introduce a spurious α_{ro}–α_{ox} correlation.

Combining the results shown in Figures 3 and 4, we can conclude that, over a range as wide as 10^5 for the ratio of radio to optical emission, there is a definite correlation between the presence and the strength of radio emission and X-ray emission. However, it is also clear from the dispersion of the points in Figures 3*a* and 4 that this correlation has only a *statistical* meaning and cannot be used simply to predict the X-ray emission of single objects.

The existence of a definite correlation between α_{ro} and α_{ox} requires some caution in discussing the $\Psi(\alpha_{ox})$ distribution of quasars originally discovered through their radio emission. In calculating the maximum likelihood estimate of the α_{ox} distribution, Avni *et al.* (1980) made use of the basic assumption that α_{ox} is independent of all other properties of the quasars which influence their selection. Since α_{ox} is now found to correlate with α_{ro}, our sample of radio selected quasars may no longer be a truly random sample of the α_{ox} distribution. This is in fact supported by a comparison of our α_{ro} distribution for radio detected quasars shown in Figure 2 with the $\Psi(R)$ distributions for optically selected and radio selected quasars shown by Fanti *et al.* (1977) and Sramek and Weedman (1980). Our α_{ro} distribution is substantially deficient in objects with $\alpha_{ro}<0.55$ when compared to the complete samples analyzed by the previous authors.

Since the data shown in Figure 4 indicate a strong correlation between α_{ro} and α_{ox}, this introduces a bias in the $\Psi(\alpha_{ox})$ and $G(<\alpha_{ox})$ distributions for radio-loud quasars shown in Figure 3. Specifically, the deficiency of radio-loud quasars with $0.35<\alpha_{ro}<0.55$ in our X-ray study leads to a corresponding deficiency of radio-loud quasars with α_{ox} predominantly in the range $1.4\lesssim\alpha_{ox}\lesssim 1.7$. This effect does not invalidate our conclusion via the modified K-S test or the $\alpha_{ox}^{\rm eff}$ calculation that the radio-loud quasars are relatively more luminous in X-rays than the radio-quiet quasars. However, the existence of more radio-loud quasars with $\alpha_{ox}\gtrsim 1.4$ will cause the integral function for radio-loud quasars in Figure 3*b* to rise less rapidly. This in turn implies that the average ratio of l_x/l_o for *all* radio-loud quasars will be somewhat less than the computed factor of 3 times higher than the same ratio for radio-quiet quasars. A more quantitative analysis of this effect will require X-ray observations of complete samples of radio-loud quasars.

c) *Correlation of α_{ox} with the Optical Luminosity and/or Redshift*

The same statistical analysis which we have described in the previous section (construction of the maximum likelihood probability distributions for α_{ox} and then comparison of these distributions through the modified K-S test and the computation of $\alpha_{ox}^{\rm eff}$) has been applied to search for correlations of α_{ox} with l_o (2500 Å) and redshift for the radio-quiet quasars, which do not suffer of any bias with respect to their X-ray properties. Dividing these quasars into two subsamples as a function of optical luminosity ($\log l_o^{\rm crit}=31.40$) and as a function of redshift ($z^{\rm crit}=1.00$), we find that in both cases the modified K-S test suggests a possible difference (levels of confidence 5×10^{-2} and 4×10^{-2}, respectively) between the distributions of α_{ox}. The $\alpha_{ox}^{\rm eff}$ also indicates a difference between the two distributions but of lesser significance (level of confidence $\sim$10%). The average value of α_{ox} may be larger (or, equivalently, the ratio of X-ray to optical luminosity smaller) for quasars at higher redshift and higher intrinsic optical luminosity. However, we cannot exclude the possibility that only one of these two correlations is real, with the second one being a consequence of the strong correlation which is present in our sample between the sampled region of the optical luminosity function and the redshift. Only future observations of a larger number of objects, covering wider regions of the luminosity function at any given redshift, can resolve this problem. These results are summarized in Table 2.

In view of the result discussed in the previous section, we have analyzed the correlation of α_{ox} with l_o and z for

TABLE 2

STATISTICAL RESULTS FOR QUASAR SUBSAMPLES

Sample	Number of Objects/Detections	Range in $\log l_o$ or z	$\alpha_{ox}^{\rm eff}\pm\sigma$	Probability from Modified K-S
Total	107/79	...	1.32 ± 0.03	
Radio loud (all)	62/59	...	1.27 ± 0.03	
Radio quiet (all)	45/20	...	$1.46^{+0.05}_{-0.07}$	5.0×10^{-4}
Radio quiet (low z)	16/13	$z<1.0$	$1.35^{+0.05}_{-0.08}$	4.0×10^{-2}
Radio quiet (high z)	29/7	$z>1.0$	$1.62^{+0.08}_{-0.16}$	
Radio quiet (low l_o)	22/13	$\log l_o<31.4$	$1.37^{+0.05}_{-0.08}$	5.0×10^{-2}
Radio quiet (high l_o) ...	23/7	$\log l_o>31.4$	$1.62^{+0.08}_{-0.16}$	

the radio-loud quasars separately, and we find respective levels of confidence of 5×10^{-3} and 11×10^{-2}. This suggests a possible dependence of α_{ox} on l_o rather than on z, but should be treated with caution given the previously discussed bias in our radio-loud sample.

We have considered the possibility that the difference between radio-loud and radio-quiet quasars is due to differences in their l_o and z distributions. A K-S test shows that the l_o distributions for the radio-loud and radio-quiet samples are similar, whereas the z distributions are not (the radio-loud sample has proportionately more low-z quasars). The absence of a strong dependence of α_{ox} on z for the radio-loud quasars we have observed suggests that the difference in redshift distributions does not significantly affect our results.

d) The Hardness Ratio of Bright X-Ray Quasars

One possible explanation for the suggested change of α_{ox} with redshift is that our use of an average $\alpha_x \approx 0.5$ for computing fluxes and luminosities is invalid. Table 3 shows how the ratio of the true to estimated monochromatic luminosity at 2 keV at the source depends on z and α_x. The IPC effective area as a function of energy and the energy resolution function have been taken into account in generating this table. These values are computed assuming a hydrogen column density $N_{\rm H}=3\times10^{20}$ cm^{-2} in the Galaxy, with no intrinsic low-energy cutoff at the source. It is clear from Table 3 that, in order to explain the nominal difference of a factor ~5 (corresponding to $\Delta\alpha_{ox}\approx0.27$) between redshift 0.5 and 2.0, we would require an average energy spectral slope $\alpha_x \gtrsim 2.0$. At present the IPC cannot be used to obtain reliable quantitative spectral fits, although calibrations presently under way should eventually remedy this situation. Therefore, we have investigated the possibility of a spectral index $\alpha_x \gtrsim 2$ by using a hardness ratio as a relative indicator of the spectral slope. By calculating the hardness ratio for various IPC gains within the permissible range, we estimate the uncertainty in the hardness ratio due to the uncertainty in the gain as no more than 20%. For 27 quasars, 21 radio-loud and six radio-quiet, with more than 100 net counts and within 5′ of the center of the IPC field of view, we have computed the hardness ratio, defined as the ratio of the net counts in the energy range 1.2–3.0 keV to the net counts from 0.5–1.2 keV. Figure 5 shows the hardness ratio distribution; the arrow shows the hardness ratio obtained from an IPC observation of 3C 273 made by the Columbia X-ray group. A simultaneous measurement with the Monitor Proportional Counter gave a best fit slope $\alpha_x=0.4$ in the energy range 2–15 keV, consistent with the best fit slope $\alpha_x=0.52\pm0.06$ in the energy range 2–9 keV measured with the *HEAO* A2 experiment (Worrall *et al.* 1979). This figure, which shows a pronounced peak around a value corresponding to $\alpha_x\approx$ 0.4–0.5, provides no evidence that changes of α_{ox} with redshift are due to a steep X-ray spectrum with $\alpha_x\approx2.0$. It is also interesting that the slope corresponding to the peak of the distribution coincides with the measured slope of the X-ray background around a few keV (see § IV). The relevance of this discussion will be greatly strengthened when more data are available for radio-quiet quasars.

TABLE 3

RATIO OF $l(2\text{ keV})_{\rm true}/l(2\text{ keV})_{\rm estimated}$ AS A FUNCTION OF REDSHIFT AND ENERGY SPECTRAL SLOPE ($N_{\rm H}=3\times10^{20}$)

	α_x			
z	0.0	0.5	1.0	2.0
0.5.....	1.03	1.00	0.88	0.47
1.0.....	0.90	1.00	1.02	0.72
2.0.....	0.72	1.00	1.27	1.43
3.0.....	0.62	1.00	1.48	2.25

Figure 6 shows the weighted average of the hardness ratio in four different redshift bins. In computing these averages, we weighted each individual object by the inverse of $\sigma_i^2=\sigma_{\rm int}^2+\sigma_{{\rm meas},i}^2$, where $\sigma_{\rm int}$ is the intrinsic dispersion of the distribution of the hardness ratio and $\sigma_{{\rm meas},i}$ is the statistical standard deviation associated with the ith measurement. We have estimated the value of $\sigma_{\rm int}^2$ as $\sigma_{\rm obs}^2-\bar{\sigma}_{\rm meas}^2$, where $\sigma_{\rm obs}$ is the observed standard deviation of the distribution and $\bar{\sigma}_{\rm meas}^2$ is the average of the individual $\sigma_{{\rm meas},i}$. Our 27 sources provide no evidence of change of the hardness ratio with redshift up to $z\approx2.5$, thus implying no significant steepening of the "average" spectrum up to $E\approx10$ keV at the source. Also, we do not see any significant evidence of excess of low energy photons caused by a spectral steepening at around 1–2 keV. Such a steepening (with α_x changing

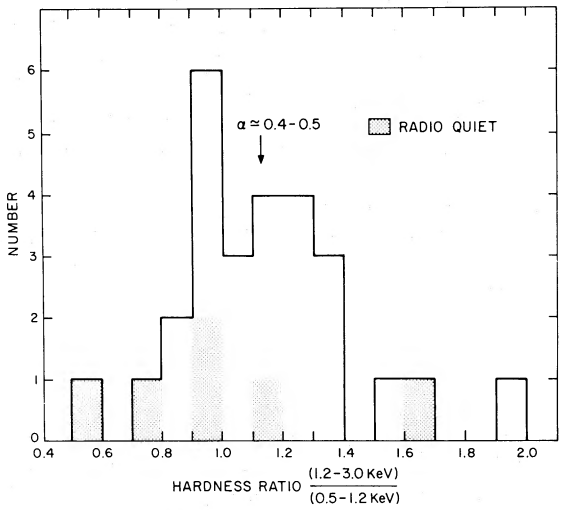

FIG. 5.—Distribution of the hardness ratio for 27 quasars with more than 100 net counts. The hardness ratio is defined as the ratio of the net counts in the energy range 1.2–3.0 keV to the net counts from 0.5–1.2 keV.

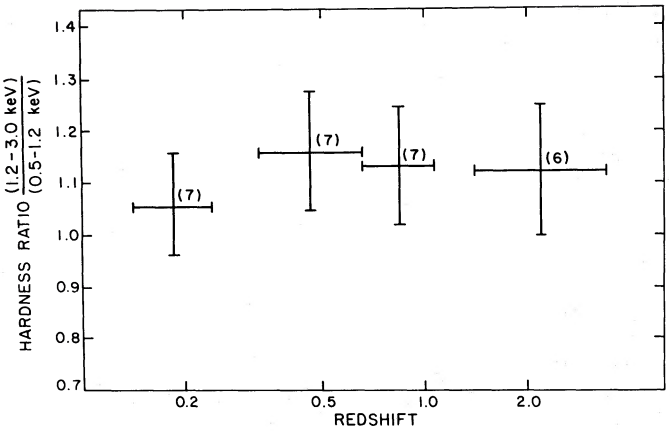

FIG. 6.—Weighted average of the hardness ratio in four different redshift bins. The number of objects in each bin is indicated.

from 2.2 below 2 keV to 0.3 above 2 keV) has been recently reported by Riegler, Agrawal, and Mushotzky (1979) for the BL Lac object PKS 0548−322.

IV. THE X-RAY BACKGROUND AND THE NUMBER OF FAINT QUASARS

It was noted in Paper I that, if the X-ray properties of the ∼30 quasars for which X-ray data were then available were typical of all QSOs, quasars could contribute most of the diffuse X-ray background. It was also pointed out that the first sample of quasars was biased by a high fraction of radio-loud objects. The differences in X-ray properties discussed above in § III between radio-loud and radio-quiet quasars, and between low-redshift and high-redshift quasars, allow us to make a more precise estimate of the total contribution of quasars to the X-ray background, to compare this estimate with the results of high sensitivity X-ray surveys (Giacconi *et al.* 1979), and to set limits to the maximum number of faint quasars. These new data also allow us to remove the previous inconsistency among X-ray observations of quasars, quasar optical counts, and deep survey X-ray results (see Cavaliere *et al.* 1980 for a similar discussion of this point).

Following the notations used in Paper I and in Avni *et al.* (1980), we define an "effective" α_{ox} as the spectral index corresponding to the average ratio of X-ray to optical luminosity:

$$\alpha_{ox}^{\rm eff} = -\frac{\log\langle l_{2\ \rm keV}/l_{2500\ \text{Å}}\rangle}{2.605}, \qquad (3)$$

where $2.605 = \log(\nu_{2\ \rm keV}/\nu_{2500\ \text{Å}})$. Table 2 gives the values of the effective α_{ox} computed for different subsamples. The corresponding values of $l_{2\ \rm keV}/l_{2500\ \text{Å}}$, weighted by the appropriate percentage of objects in each of the subsamples, can be used to obtain an average $\alpha_{ox}^{\rm eff}$ ($\langle\alpha_{ox}^{\rm eff}\rangle$). Given the steep slope of quasar optical counts (Green and Schmidt 1978; Braccesi *et al.* 1980), most of the observable X-ray flux will come from quasars at faint magnitudes, for which the redshift distribution is poorly known. From the data published by Braccesi *et al.* (1980) and Bolton and Savage (1978) we estimate that at ∼19–20 mag about 75% of the optically selected quasars have $z>1$. With the additional information that ∼10% of the optically selected QSOs are radio-loud (Fanti *et al.* 1977; Sramek and Weedman 1978), we obtain $\langle\alpha_{ox}^{\rm eff}\rangle \approx 1.45$.

Using the optical counts as a normalization, we can compute the expected X-ray flux from QSOs brighter than any limiting flux $S_{1-3\ \rm keV}^{\rm lim}$ by a double integral over the optical counts and the α_{ox} distribution:

$$s_{2\ \rm keV} = A(z_{\rm eff},\alpha_o,\alpha_x)\int_{m_B^{\rm min}}^{m_B^{\rm Max}} 10^{-19.38-0.4m_B}\frac{dn}{dm_B}dm_B \times \int_{-\infty}^{\alpha_{ox}^{\rm Max}(m_B,S_{1-3\ \rm keV}^{\rm lim})} f(\alpha_{ox})10^{-2.605\alpha_{ox}}d\alpha_{ox}, \qquad (4)$$

where $s_{2\ \rm keV}$ is the expected monochromatic flux at 2 keV; $A(z_{\rm eff},\alpha_o,\alpha_x)=(2500/4409)^{\alpha_o}(1+z_{\rm eff})^{\alpha_o-\alpha_x}\approx 1$ is a function of the assumed energy slopes at optical and X-ray frequencies; $z_{\rm eff}$ is the redshift for the typical QSO contributing to the X-ray background (taken as ∼1.5 here); dn/dm_B is the assumed optical number counts between $m_B^{\rm min}$ and $m_B^{\rm Max}$; $10^{-19.38-0.4m_B}$ is the monochromatic optical flux at 4409 Å of an object with magnitude m_B; $f(\alpha_{ox})$ is the probability distribution of α_{ox}; and $\alpha_{ox}^{\rm Max}(m_B,S_{1-3\ \rm keV}^{\rm lim})$ is the maximum value of α_{ox} that an object of magnitude m_B can have in order to have an X-ray flux $S_{1-3\ \rm keV}^{\rm lim}$.

In a similar way, we can compute the expected number of QSOs brighter than any limiting flux $S_{1-3\ \rm keV}^{\rm lim}$:

$$N(>S_{1-3\ \rm keV}^{\rm lim}) = \int_{m_B^{\rm min}}^{m_B^{\rm Max}}\frac{dn}{dm_B}dm_B \times \int_{-\infty}^{\alpha_{ox}^{\rm Max}(m_B,S_{1-3\ \rm keV}^{\rm lim})} f(\alpha_{ox})\,d\alpha_{ox}. \qquad (5)$$

If we make the reasonable assumption (Fig. 3*a*) that we can approximate the α_{ox} probability distribution with a Gaussian distribution, the double integrals of equations (4) and (5) can be evaluated analytically. Assuming the optical $\log N$–m given by Braccesi *et al.* (1980), [$\log N(m_B)=2.16(m_B-18.33)/2.5$ objects per square degree] and integrating it up to $m_B=20.0$, we find that the total ($S^{\lim}_{1-3\ \mathrm{keV}}\to 0$) monochromatic flux at 2 keV from the quasars brighter than $m_B=20$ is $\sim 30\%$ of the observed background (Schwartz 1978). At the limit of the *Einstein* deep surveys ($S^{\lim}_{1-3\ \mathrm{keV}}\approx 2.6\times 10^{-14}$ ergs cm^{-2} s^{-1}), the contribution of quasars brighter than $m_B\simeq 20.0$ would be approximately 25% of the observed background and the expected number is ~ 13 per square degree, in excellent agreement with the number counts of extragalactic X-ray sources discussed by Giacconi *et al.* (1979).

If we extrapolate the integration along the optical $\log N$–m without changing its slope and assume the same distribution of α_{ox}, we find that the quasars at $m_B\approx 21.2$ would give $\sim 100\%$ of the extragalactic diffuse X-ray background, and discrete sources accounting for $\sim 65\%$ of the background would be seen at the deep survey limits. This last figure is in contradiction with the observed percentage of $(26\pm 11)\%$ (Giacconi *et al.* 1979). Although the uncertainties in our estimates may be as high as a factor two, this result seems to indicate that either as we go to fainter magnitudes the ratio l_x/l_o is decreasing by even more than our weighted average above has taken into account or the slope of the optical counts becomes much flatter at $m_B\approx 20$. The presence of such a flattening has been suggested by Bohuski and Weedman (1979) as well as by Vaucher and Weedman (1980). Independent confirmation comes from recent optical studies by Kron (1980). Analyzing a color-color diagram ($U-J$ versus $J-F$) for stellar objects in the selected Area 68, he finds ~ 6–9 candidate quasars in 130 arcmin^2 (~ 200 per square degree) at the limits $U\leq 23$, $J\leq 23.5$, $F\leq 22.5$. Even more stringent limits on the density of faint quasars have been obtained by Bahcall and Soneira (1981). By fitting a detailed model of the stellar content of the Galaxy to the counts of faint stars, they obtain an upper limit of ~ 50 quasars per square degree down to $m_B\approx 22.5$. Both these estimates imply a quite substantial flattening of the slope of the $\log N$–m when compared with the surface density of ~ 25 quasars per square degree at $m_B\sim 20$ implied by the $\log N$–m given by Braccesi *et al.* (1980). (After this work had been completed, we received a preprint from Bonoli *et al.* 1980 which presents data showing a flattening in the optically selected quasar counts around $m_B\sim 20$. This is essentially caused by the discovery of the extended nature of many of the faint blue objects previously classified as quasars.)

The presence of this turnover in the surface density of faint quasars, which is now suggested both from optical and X-ray data, is an important constraint to the evolutionary laws for quasars. It is straightforward to show that it is not possible to reproduce such a turnover with a *pure* density evolution of the local luminosity function as derived from complete samples of optically selected QSOs. In the framework of density evolution, we have to invoke luminosity-dependent density evolution (stronger evolution for higher luminosities) if we wish to fit both the steep counts up to $m_B\approx 20$ and the flattening at fainter magnitudes. Alternatively, pure luminosity evolution [$L(z)=L_0e^{k\tau}$, $\tau=z/(1+z)$ in $q_0=0$ models] which successfully describes magnitude and redshift distributions of complete samples (Mathez 1976, 1978) gives a very natural explanation for the suggested flattening.

V. IMPLICATIONS OF X-RAY OBSERVATIONS FOR QUASAR EMISSION MODELS

In view of the preceding results, an extremely simplified and qualitative scenario for the X-ray emission can be depicted.

a) In all of the quasars (both radio-loud and radio-quiet) there is a central "energy machine" which provides at least part of the optical and X-ray emission. The average α_{ox} slope should be similar to that observed for our sample of radio quiet QSOs ($\sim 1.5\pm 0.1$). Any mechanism aimed at explaining this emission should contain one or more variable parameters which can produce the large observed dispersion in l_x/l_o. Such parameters can be easily identified, for example, in the nonrelativistic Compton scattering model proposed by Katz (1976), in which the slope α_{ox} is determined by the radius and temperature of the Comptonizing cloud of hot gas.

b) In radio-loud quasars an additional mechanism for producing X-rays (synchrotron or synchro-Compton) is required in order to explain the higher observed average ratio of l_x/l_o. Since it is likely that the "radio-quiet mechanism" also contributes, we expect that the intrinsic slope of this second component is even flatter than the observed α_{ox} for radio-loud QSOs. Recent jet models proposed by Scheuer and Readhead (1979) and by Blandford and Königl (1979) explain the difference between radio-loud and radio-quiet QSOs as due essentially to geometric effects (angle between the line of sight and the direction of the jet). In the context of these models at least part of the X-ray emission would be connected with the jet and would quite likely be produced at its very beginning near the nucleus. In this case the X-ray emission from the jet would be closely related to the optical continuum emission, while the strong radio emission probably occurs in a physically distinct, outlying region.

If we denote by K the percentage of the total optical emission due to this second mechanism (i.e., that associ-

ated with radio emission), the radio-quiet QSOs ($K \ll 1$) are dominated by the first mechanism which should be responsible for their small optical polarization (Stockman and Angel 1978; Angel and Stockman 1980), their smaller degree of variability compared to radio-loud QSOs (Bonoli *et al.* 1979), and their relatively steep α_{ox}. At the opposite extreme ($K \sim 1$), the objects have high optical variability (OVV), high level of radio and optical polarization, and flatter slope α_{ox}. Two of these extreme quasars (3C 446 and 3C 279) are in our sample, and they have the two smallest observed α_{ox} (0.91 and 0.97, respectively). For intermediate K we expect intermediate properties with respect to optical polarization, variability, and α_{ox}. This range of values for K might be responsible for the observed distribution of α_{ro} versus α_{ox} shown in Figure 4.

On the basis of this two-mechanism scenario we expect X-ray variability to be stronger and more frequent in radio-loud than in radio-quiet QSOs, and possibly correlated in strength and in time with optical variability. In order to check this suggested correlation, a program of simultaneous optical and X-ray observations of a sample of about 10 objects is in progress at the Center for Astrophysics.

A possible difficulty with this scenario relates to the question of the equivalent widths of the permitted lines in the OVV quasars compared to the non–OVV quasars. Specifically, the enhanced continuum emission in the OVVs is assumed to be due to the favorable orientation of the observer with respect to the jet. This predicts reduced equivalent widths for the permitted lines which are likely to be unaffected by the jet orientation. Smith and Wright (1980), in comparing samples of radio-loud and radio-quiet QSOs, find that large differences in the ratio of radio to optical luminosity are not accompanied by an obvious corresponding change in the equivalent width of the emission lines. Further optical observations of the objects in Table 1 are needed to test this question. These in turn will affect the validity of the jet model as the explanation of the extra component which our data require for radio-loud quasars.

VI. SUMMARY

From the analysis of a sample of 107 observed quasars we have derived some properties of their X-ray emission which should be explained by any model of the energy production mechanisms in such objects.

In summary, we have found that:

i) A large fraction (if not all) of the quasars are X-ray emitters with X-ray luminosities ranging over a factor of 10^5 (from $\sim 5 \times 10^{42}$ to $\sim 5 \times 10^{47}$ ergs s^{-1}).

ii) Their X-ray luminosity is roughly proportional to the optical luminosity, but the dispersion in l_x/l_o is large (a range of about a factor 10 covers 68% of the objects, while the total observed range corresponds to a factor ~ 300).

iii) The average energy spectral slope between optical and X-ray frequencies is ~ 1.4–1.5.

iv) For the radio-loud QSOs ($\alpha_{ro} \geq 0.35$) there is strong evidence that, for a given optical luminosity, their X-ray luminosity is up to 3 times stronger than for the radio-quiet QSOs (their α_{ox} is smaller).

v) Within our sample of radio-loud QSOs there is a correlation between α_{ro} and α_{ox} in the direction that stronger radio emission (higher α_{ro}) is associated with stronger X-ray emission (smaller α_{ox}).

vi) For both radio-quiet and radio-loud QSOs there is evidence that the average value of l_x/l_o either might be a function of redshift (l_x/l_o decreasing with increasing redshift) or might change with optical luminosity (l_x/l_o decreasing with increasing l_o). The lowest average value of l_x/l_o is for radio quiet, high redshift quasars, for which our detection rate is seven out of 29.

vii) The hardness ratio distribution for 27 bright X-ray quasars (mainly radio-loud) is peaked around a value corresponding to $\alpha_x \approx 0.4$–0.5, in good agreement with the observed slope of the X-ray background in the energy range of a few keV.

viii) There is no evidence for change of the hardness ratio with redshift up to $z \approx 2.5$.

ix) Taking into account the differences between radio-loud and radio-quiet and between low-redshift and high-redshift quasars, we estimate that $\sim 30\%$ of the observed X-ray background can be contributed by quasars brighter than $m_B \approx 20$.

x) The optical $\log N$–m_B relation can not be extrapolated with the observed steep slope much beyond $m_B \approx 20$ without exceeding the observed X-ray background. This situation supports the picture in which luminosity evolution, rather than pure density evolution, describes the quasar behavior as a function of redshift.

While this paper was in final stages of preparation we received a preprint from Ku and Helfand which contains additional *Einstein* observations of quasars carried out by the Columbia X-ray Group. In general the results of their analysis lead to conclusions similar to our own. However, their analysis which is based on the assumption of Gaussian distributions of α_{ox} for various quasar subsets is less general than our nonparametric analysis. The result is that they derive uncertainties in the average α_{ox} for the various subsets which may be significantly underestimated if the distributions are not actually Gaussian.

We acknowledge useful discussions with Drs. S. Murray, M. Elvis, and E. Feigelson. We thank K. Gilleece for her constant efforts in preparing this manuscript for publication. This research was sponsored under NASA contract NAS8-30751. G. Z. acknowledges support by a European Space Agency fellowship, and Y. A. by a USA–Israel BSF grant.

APPENDIX

A MODIFIED VERSION OF THE KOLMOGOROV-SMIRNOV (K-S) TEST

The K-S test is a well known test for comparing two different samples of objects to determine if they come from the same population. The application of this test is extremely simple. Let n_1 and n_2 be the number of objects in the two samples, and let α be the variable whose distribution is being compared. The test considers the maximum deviation (D) between the two integral probability distributions $G(<\alpha)$ of the two samples, where $G(<\alpha^*)$ is the fraction of the observations with $\alpha<\alpha^*$ ($D=\max|G_1(<\alpha)-G_2(<\alpha)|$). For large samples the quantity

$$\mathrm{KS}=4D^2\frac{n_1 n_2}{(n_1+n_2)} \tag{A1}$$

has a sampling distribution approximated by the χ^2 distribution with two degrees of freedom. Therefore, the usual χ^2 tables give the level of confidence at which we can reject the null hypothesis (i.e., that the two samples are drawn from the same population).

In our actual case, there are at least two reasons for which we cannot straightforwardly apply the test in its usual formulation:

1. When we divide the total sample into different subsamples (as, for example, radio-quiet QSOs at low redshift and at high redshift), there are cases in which we are no longer dealing with "large" samples.
2. Our X-ray observations have resulted not only in detections but also in a number of X-ray flux upper limits, or α_{ox} lower limits. It is clear that, if we neglect these lower limits in the application of any statistical test, we will not have made full use of our data set and the results obtained in this way may, therefore, be in error.

In order to extend the applicability of the K-S test to our case we have used the following procedure:

i) Let us denote by P the property of our objects for which we want to study the possible correlation with the variable α. In actual cases in this paper P is redshift, or optical luminosity, or radio to optical ratio of the individual quasars.

ii) We assume (null hypothesis) that P and α are not correlated, and compute the maximum likelihood probability distribution in α for the total sample (Avni *et al.* 1980), taking into account any lower limits in α.

iii) By using a Monte Carlo calculation we construct a distribution both of α and of lower limits for α for the two samples under examination ($P<P^{\mathrm{crit}}$ and $P\geq P^{\mathrm{crit}}$). In order to decide if the kth value of the randomly generated α (α_k^{rand}) should be considered as a detection or a lower limit, we compare this value with the

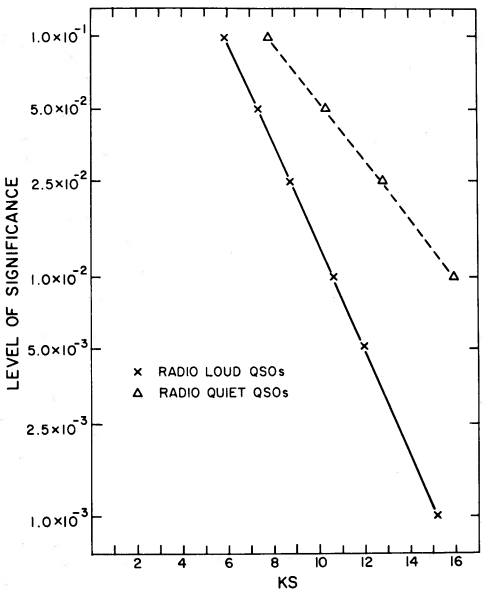

FIG. 7.—KS distribution from the modified K-S test versus level of significance for rejection of the null hypothesis for two different samples. The results shown here for the two samples refer to the correlation between α_{ox} and optical luminosity ($\log l_o^{\mathrm{crit}}=31.4$). The solid line shows the expected KS distribution in the absence of upper limits. Our analysis of the radio-loud sample versus l_o yielded a KS value of 11.9, while the radio-quiet sample yielded a KS value of 10.8. These KS values correspond to the confidence levels stated in the text.

maximum α that the kth object could have determined in its actual observation ($\alpha_k^{\rm lim}$). If $\alpha_k^{\rm rand} \leq \alpha_k^{\rm lim}$, we have a detection at $\alpha_k^{\rm rand}$; if $\alpha_k^{\rm rand} > \alpha_k^{\rm lim}$, we have a lower limit at $\alpha_k^{\rm lim}$.

iv) We compute the maximum likelihood probability distribution for the two randomly generated samples and the resulting KS (eq. [A1]) from the application of the K-S test on these "corrected" distributions.

v) By iterating the previous procedure a sufficient number of times, we obtain the distribution of K-S which is appropriate for the pair of samples being examined.

vi) At this point we compare the observed value of KS with the distribution obtained from the Monte Carlo calculation and read the level of significance at which the null hypothesis can be rejected.

Figure 7 shows the results obtained for two of the analyzed pairs of samples along with the results expected in the absence of upper limits. The KS distribution obtained for the radio-loud QSOs for which we have only three upper limits out of 62 observations is practically indistinguishable from the expected distribution. However, as we go to a sample with a higher fraction of upper limits (the radio quiet sample), the difference from the expected distribution becomes larger. The presence of upper limits tends to reduce the statistical significance of an observed value of KS (by as much as a factor of 5 for our specific situation).

REFERENCES

Adam, G. 2978, *Astr. Ap. Suppl.*, **31**, 151.
Angel, J. R. P., and Stockman, H. S. 1980, *Ann. Rev. Astr. Ap.*, in press.
Argue, A. M., *et al.* 1974, *M.N.R.A.S.*, **168**, 1P.
Avni, Y., Soltan, A., Tananbaum, H., and Zamorani, G. 1980, *Ap. J.*, **238**, 800.
Bahcall, J. N., and Soneira, R. M. 1981, *Ap. J.*, **245**, in press.
Bergamini, R., *et al.* 1973, *Astr. Ap.*, **23**, 195.
Blandford, R. D., and Konigl, A. 1979, *Ap. J.*, **232**, 34.
Bohuski, T. J., and Weedman, D. W. 1979, *Ap. J.*, **231**, 653.
Bolton, J. G., and Savage, A. 1978, in *IAU Symposium 79, The Large Scale Structure of the Universe*, ed. M. S. Longair and J. Einasto (Dordrecht: Reidel), p. 295.
Bonoli, F., Braccesi, A., Federici, L., Zitelli, V., and Formiggini, L. 1979, *Astr. Ap. Suppl.*, **35**, 391.
Bonoli, F., Braccesi, A., Marano, B., Merighi, R., and Zitelli, V. 1980, *Astr. Ap. Letters*, submitted.
Braccesi, A., Zitelli, V., Bonoli, F., and Formiggini, L. 1980, *Astr. Ap.*, **85**, 80.
Burbidge, G. R., Crowne, A. M., and Smith, H. E. 1977, *Ap. J. Suppl.*, **33**, 113.
Cavaliere, A., Danese, L., DeZotti, G., and Franceschini, A. 1980, preprint.
Fanti, C., Fanti, R., Lari, C., Padrielli, L., van der Laan, H., and de Ruiter, H. 1977, *Astr. Ap.*, **61**, 487.
Fanti, R., Formiggini, L., Lari, C., Padrielli, L., Katgert-Merkelijn, J. K., and Katgert, P. 1973, *Astr. Ap.*, **23**, 161.
Giacconi, R., *et al.* 1979, *Ap. J.* (*Letters*), **234**, L1.
Green, R. F., and Schmidt, M. 1978, *Ap. J.* (*Letters*), **220**, L1.
Grindlay, J. E., Steiner, J. E., Forman, W. R., Canizares, C. R., and McClintock, J. E. 1980, *Ap. J.* (*Letters*), **239**, L43.
Heiles, C. 1975, *Astr. Ap. Suppl.*, **20**, 37.
Jauncey, D. L., Wright, A. E., Peterson, B. A., and Condon, J. J. 1978*a*, *Ap. J.* (*Letters*), **219**, L1.
_____. 1978*b*, *Ap. J.* (*Letters*), **221**, L109.
Katz, J. I. 1976, *Ap. J.*, **206**, 910.
Kembhavi, A., and Fabian, A. 1980, *IAU Symposium on Origin of Cosmic Rays*, held in Bologna 1980 June.
Kendall, M. G., and Stuart, A. 1961, *The Advanced Theory of Statistics*, Vol. **2** (New York: Hafner Publishing Co.).
Kron, R. G. 1980, in *Two Dimensional Photometry* (*ESO Workshop*), ed. P. O. Lindblad and H. van der Laan, Geneva.
Ku, W. H. M. 1979, IAU Joint Discussion on Extragalactic High Energy Astrophysics, IAU General Assembly, Montreal, to be published in *Highlights of Astronomy*, ed. H. van der Laan.
MacAlpine, G. M., and Lewis, D. W. 1978, *Ap. J. Suppl.*, **36**, 587.
MacAlpine, G. M., Lewis, D. W., and Smith, S. B. 1977, *Ap. J. Suppl.*, **25**, 203.
MacAlpine, G. M., Smith, S. B., and Lewis, D. W. 1977, *Ap. J. Suppl.*, **35**, 197.
Margon, B. 1977, *Ap. J.* (*Letters*), **211**, L5.
Mathez, G. 1976, *Astr. Ap.*, **53**, 15.
_____. 1978, *Astr. Ap.*, **68**, 17.
Nieto, J. L. 1978, *A. J.*, **83**, 1141.
Osmer, P. S., and Smith, M. G. 1977*a*, *Ap. J.*, **213**, 607.
_____. 1977*b*, *Ap. J.* (*Letters*), **215**, L47.
_____. 1977*c*, *Ap. J.* (*Letters*), **217**, L73.
Peterson, B. A., Jauncey, D. L., Wright, A. E., and Condon, J. J. 1978, *Ap. J.* (*Letters*), **222**, L81.
Riegler, G. R., Agrawal, P. C., and Mushotzky, R. F. 1979, *Ap. J.* (*Letters*), **233**, L47.
Sandage, A. R. 1961, *Ap. J.*, **133**, 355.
Scheuer, P. A. G., and Readhead, A. C. S. 1979, *Nature*, **277**, 182.
Schmidt, M. 1968, *Ap. J.*, **151**, 393.
_____. 1972, *Ap. J.*, **176**, 273.
Schwartz, D. A. 1978, Proc. IAU/COSPAR Symposium on X-ray Astronomy, Innsbruck, Austria.
Smith, M. G., and Wright, A. E. 1980, *M.N.R.A.S.*, in press.
Sramek, R. A., and Weedman, D. W. 1978, *Ap. J.*, **221**, 468.
_____. 1980, *Ap. J.*, **238**, 435.
Stockman, H. S., and Angel, J. R. P. 1978, *Ap. J.* (*Letters*), **220**, L67.
Tananbaum, H., *et al.* 1979, *Ap. J.* (*Letters*), **234**, L9 (Paper I).
Vaucher, B. G., and Weedman, D. W. 1980 preprint.
Wills, D., and Lynds, R. 1978, *Ap. J. Suppl.*, **36**, 317.
Worrall, D. M., Mushotzky, R. F., Boldt, E. A., Holt, S. S., and Serlemitsos, P. J. 1979, *Ap. J.*, **232**, 683.
Wright, A. E., Peterson, B. A., Jauncey, D. L., and Condon, J. J. 1978, *Ap. J.* (*Letters*), **226**, L61.

Y. Avni: The Weizmann Institute of Science, Department of Nuclear Physics, Rehovot, Isreal

J. J. Condon: Physics Department, Virginia Polytechnic Institute and State University, 325 Robeson Hall, Blacksburg, VA 24061

J. P. Henry, T. Maccacaro, H. Tananbaum, and G. Zamorani: Harvard-Smithsonian Center for Astrophysics, 60 Garden Street, Cambridge, MA 02138

J. Liebert, J. Stocke, P. A. Strittmatter, and R. J. Weymann: Steward Observatory, University of Arizona, Tucson, AZ 85721

M. G. Smith: Royal Observatory, Blackford Hill, Edinburgh, UK

A. Soltan: N. Copernicus Astronomical Center, ul. Bartycka 18, 00-716-Warszawa, Poland